

# ALMA reveals a warm and compact starburst around a heavily obscured supermassive black hole at $z = 4.75$

R. Gilli<sup>1</sup>, C. Norman<sup>2,3</sup>, C. Vignali<sup>4,1</sup>, E. Vanzella<sup>1</sup>, F. Calura<sup>1</sup>, F. Pozzi<sup>4,1</sup>, M. Massardi<sup>5</sup>, A. Mignano<sup>5</sup>, V. Casasola<sup>5</sup>, E. Daddi<sup>6</sup>, D. Elbaz<sup>6</sup>, M. Dickinson<sup>7</sup>, K. Iwasawa<sup>8</sup>, R. Maiolino<sup>9</sup>, M. Brusa<sup>4,1</sup>, F. Vito<sup>4,1</sup>, J. Fritz<sup>10</sup>, A. Feltre<sup>11,12</sup>, G. Cresci<sup>1</sup>, M. Mignoli<sup>1</sup>, A. Comastri<sup>1</sup> and G. Zamorani<sup>1</sup>

<sup>1</sup> INAF – Osservatorio Astronomico di Bologna, via Ranzani 1, 40127 Bologna, Italy  
e-mail: roberto.gilli@oabo.inaf.it

<sup>2</sup> Department of Physics and Astronomy, Johns Hopkins University, Baltimore, MD 21218, USA

<sup>3</sup> Space Telescope Science Institute, 3700 San Martin Drive, Baltimore, MD 21218, USA

<sup>4</sup> Dipartimento di Fisica e Astronomia, Università degli Studi di Bologna, viale Berti Pichat 6/2, 40127 Bologna, Italy

<sup>5</sup> Istituto di Radioastronomia & Italian ALMA Regional Centre, Via P. Gobetti 101, 40129 Bologna, Italy

<sup>6</sup> Laboratoire AIM, CEA/DSM-CNRS-Université Paris Diderot, Irfu/Service d'Astrophysique, CEA Saclay, Orme des Merisiers, 91191 Gif-sur-Yvette Cedex, France

<sup>7</sup> NOAO, 950 North Cherry Avenue, Tucson, AZ 85719, USA

<sup>8</sup> ICREA and Institut de Ciències del Cosmos (ICC), Universitat de Barcelona (IEEC-UB), Martí i Franquès 1, 08028 Barcelona, Spain

<sup>9</sup> Cavendish Laboratory, University of Cambridge, 19 J. J. Thomson Ave., Cambridge CB3 0HE, UK

<sup>10</sup> Sterrenkundig Observatorium, Universiteit Gent, Krijgslaan 281 S9, B-9000 Gent, Belgium

<sup>11</sup> UPMC-CNRS, UMR7095, Institut d'Astrophysique de Paris, F-75014, Paris, France

<sup>12</sup> ESO, Karl-Schwarzschild-Str 2, D-85748 Garching bei München, Germany

Received ; accepted

## ABSTRACT

We report ALMA Cycle 0 observations at 1.3mm of LESS J033229.4-275619 (XID403), an Ultraluminous Infrared Galaxy at  $z = 4.75$  in the Chandra Deep Field South hosting a Compton-thick QSO. The source is not resolved in our data at a resolution of  $\sim 0.75$  arcsec, placing an upper-limit of 2.5 kpc to the half-light radius of the continuum emission from heated-dust. After deconvolving for the beam size, however, we found a  $\sim 3\sigma$  indication of an intrinsic source size of  $0.27 \pm 0.08$  arcsec (Gaussian FWHM), which would correspond to  $r_{half} \sim 0.9 \pm 0.3$  kpc. We build the far-IR SED of XID403 by combining datapoints from both ALMA and Herschel and fit it with a modified blackbody spectrum. For the first time, we measure the dust temperature  $T_d = 58.5 \pm 5.3$  K in this system, which is comparable to what has been observed in other high- $z$  submillimeter galaxies. The measured star formation rate is  $SFR = 1020 \pm 150 M_\odot \text{ yr}^{-1}$ , in agreement with previous estimates at lower S/N. Based on the measured SFR and source size, we constrain the SFR surface density to be  $\Sigma_{SFR} > 26 M_\odot \text{ yr}^{-1} \text{ kpc}^{-2}$  ( $\sim 200 M_\odot \text{ yr}^{-1} \text{ kpc}^{-2}$  for  $r_{half} \sim 0.9$  kpc). The compactness of this starburst is comparable to what has been observed in other local and high- $z$  starburst galaxies. If the gas mass measured from previous [CII] and CO(2-1) observations at low resolution is confined within the same dust region, assuming  $r_{half} \sim 0.9 \pm 0.3$  kpc, this would produce a column density of  $N_H \sim 0.3 - 1.1 \times 10^{24} \text{ cm}^{-2}$  towards the central SMBH, similar to the column density of  $\approx 1.4 \times 10^{24} \text{ cm}^{-2}$  measured from the X-rays. Then, in principle, if both gas and dust were confined on sub-kpc scales, this would be sufficient to produce the observed X-ray column density without any need of a pc-scale absorber (e.g. the torus postulated by Unified Models). We speculate that the high compactness of star formation, together with the presence of a powerful AGN, likely produce an outflowing wind. This would be consistent with the  $\sim 350 \text{ km s}^{-1}$  velocity shift observed between the Ly $\alpha$  emission and the submm lines ([CII], CO(2-1), [NII]) and with the highly-ionized Fe emission line at  $\sim 6.9 \text{ keV}$  rest-frame tentatively observed in the X-ray spectrum. Finally, our observations show that, besides the mass, star formation rate and gas depletion timescale, XID403 has also the right size to be one of the progenitors of the compact quiescent massive galaxies seen at  $z \sim 3$ .

**Key words.** galaxies: high-redshift – submillimeter: galaxies – galaxies: active – X-rays

## 1. Introduction

A major effort in observational cosmology is devoted to understand the way galaxies and supermassive black holes (BHs) at their centers grow together. Broadly speaking, a scenario is emerging (see e.g. Hopkins et al. 2008) in which both star formation and nuclear accretion might occur in two distinct modes. The bulk of the galaxies and black holes would grow their mass in a secular, smooth fashion over  $\sim \text{Gyr}$ -long timescales (Daddi et al. 2007; Cisternas et al. 2011). A minor fraction of these systems, which are nonetheless the most massive and luminous,

would instead assemble most of its mass during a few rapid bursts of activity, of the order of  $\approx 0.01$ - $0.1$  Gyr (Alexander et al. 2005). Recent results from deep multiwavelength surveys featuring far-IR data from Herschel (Nordon et al. 2010; Elbaz et al. 2011; Rodighiero et al. 2011) are confirming the distinction between the bulk of objects which are growing quietly (the so-called “main sequence”) and that turbulent minority which instead is growing in bursts and is responsible for  $\sim 10\%$  of the cosmic star formation rate density at  $z \sim 2$  (Rodighiero et al. 2011). For this last population, mergers between gas-rich galaxies are believed to trigger both vigorous star formation and ob-

scured, Eddington limited, accretion (Menci et al. 2008). AGN feedback is then supposed to heat and eventually expel the surrounding gas, quenching star formation and allowing a direct, unobscured view of the nucleus (Hopkins et al. 2008; Menci et al. 2008). As these systems run out of gas, quiescent galaxies are left with dormant BHs in their center.

Ultraluminous Infrared Galaxies (ULIRGs, Sanders & Mirabel 1996) in the local Universe and bright submillimeter galaxies (SMGs) in the distant ( $z \sim 2 - 3$ ) Universe (Blain et al. 2002) are often identified as those systems caught during their turbulent youth. Morphological studies show that most local ULIRGs do show merger signatures (Sanders & Mirabel 1996). Similarly, submillimeter galaxies often show asymmetric and disturbed morphologies (Chapman et al. 2003; Tacconi et al. 2006, 2008; Engel et al. 2010). Both populations produce stars at very high rates ( $\text{SFR} = 100\text{--}1000 M_{\odot}\text{yr}^{-1}$ ), host large reservoirs of molecular gas ( $M_{\text{gas}} \sim 10^{10} M_{\odot}$ , see Solomon & Vanden Bout 2005 for a review) and often hide heavily obscured, even Compton-thick AGN (Alexander et al. 2005; Iwasawa et al. 2011). Very recently, Wang et al. (2013b) estimated that  $\approx 20\%$  of the SMGs in the ALMA-LABOCA survey of the ECDFS (ALESS, Hodge et al. 2013) host X-ray detected AGN, most of which obscured with  $N_H > 10^{23} \text{cm}^{-2}$ . The gas consumption time ( $t_c = M_{\text{gas}}/\text{SFR}$ ) and AGN lifetime in SMGs (i.e. the time necessary to grow the black hole and reach the local  $M_{\text{BH}}/M_{\text{bulge}}$  relation, assuming Eddington rate) are estimated to be short,  $\sim 10^7$  yr. A particularly intriguing possibility is that during this short, possibly Compton-thick accretion phase, the BH provides maximum feedback on the surrounding gas through Compton heating of the galaxy ISM (Daddi et al. 2007). Very high column densities would indeed ensure that high-energy photons are Compton down-scattered and then absorbed by the ISM, which can then be efficiently heated until star formation is eventually quenched. Heavily obscured AGN in starburst systems are therefore ideal laboratories to study the co-evolution of black holes with their hosts.

The fast development of submm instrumentation will soon lead to major progresses in our understanding of BH-galaxy co-evolution up to the early Universe. The detection and identification of SMGs at  $z > 4$  is rapidly increasing (Capak et al. 2008; Schinnerer et al. 2008; Daddi et al. 2009; Walter et al. 2012; Weiß et al. 2013; Vieira et al. 2013), and hyperluminous infrared systems with SFR up to  $\sim 3000 M_{\odot}\text{yr}^{-1}$  are being discovered as early as  $z \sim 6.3$  (Riechers et al. 2013). The incidence and properties of obscured accreting black holes in these high-redshift systems has still to be properly assessed. One notable example is represented by the V-band dropout galaxy LESS J033229.4–275619 at  $z = 4.75$  (Vanzella et al. 2006). This object was detected in the GOODS-S field by both LABOCA and AzTEC with  $f_{870\mu\text{m}} = 6.3 \pm 1.2$  mJy and  $f_{1.1\text{mm}} = 3.3 \pm 0.5$  mJy, respectively. Based on these data, a total IR luminosity of  $6 \times 10^{12} L_{\odot}$  and a SFR of about  $1000 M_{\odot}\text{yr}^{-1}$  were derived (Coppin et al. 2009). Observations of the CO(2-1) transition with ATCA and of the [CII]158 $\mu\text{m}$  line with APEX revealed large reservoirs ( $10^{10} M_{\odot}$ ) of both molecular (Coppin et al. 2010) and atomic gas (De Breuck et al. 2011). Furthermore, the 4Ms Chandra observation of the ECDFS revealed the presence of a Compton-thick AGN in this source (also known as XID403; Xue et al. 2011) with a column density of  $N_H = 1.4_{-0.5}^{+0.9} \times 10^{24} \text{cm}^{-2}$  and an intrinsic, de-absorbed 2-10 keV luminosity of  $\sim 2.5 \times 10^{44}$  erg/s (Gilli et al. 2011). By means of a spectral energy distribution (SED) decomposition technique (Vignali et al. 2009; Pozzi et al. 2010), the bolometric output of the AGN was estimated to be about half

of that produced by stars (Gilli et al. 2011). XID403 therefore appears a prime interest target for further follow-up studies.

In this paper we present observations of XID403 obtained with the Atacama Large Millimeter/submillimeter Array (ALMA) in Cycle 0 and combine these data with those at other wavelengths to derive the physical properties of this system. We summarize ALMA observations in Section 2. In Section 3 we discuss the far-IR SED obtained by combining ALMA and Herschel data. In Section 4 the star formation rate properties are derived. In Section 5 we combine the far-IR data with those at other wavelengths (e.g. from the CANDELS catalog) to derive a whole SED and perform a spectral decomposition of the stellar and nuclear components. A reanalysis of the X-ray spectrum is presented in Section 6. Our results are discussed in Section 7 and the conclusions drawn in Section 8. A concordance  $\Lambda$ CDM cosmology with  $H_0 = 67 \text{ km s}^{-1} \text{ Mpc}^{-1}$ ,  $\Omega_m = 0.32$ ,  $\Omega_{\Lambda} = 0.68$  (Planck Collaboration XVI, 2013) is adopted to compute luminosities and physical sizes.

## 2. ALMA observations

We proposed continuum observation of XID403 during the first ALMA Early Science call for proposal, aiming at significantly improving over the existing LABOCA and Aztec detections. The project (2011.0.00716.S; PI R. Gilli) was classified as ‘filler observation’ and, at the end of the Cycle, got about 23 minutes (including calibration) allocated for the Band 6 continuum observations.

The target was observed on the 21st October 2012 with a  $22 \times 12$  m antenna array and maximum baseline  $\sim 400$  m and with  $4 \times 1.875$  GHz spectral windows covering the frequency range 222–238 GHz, with an averaged system temperature of  $\sim 67$  K. After averaging over the 7.5 GHz band the mean effective frequency for the continuum observations is 230 GHz. The time on source was  $\sim 3$  min and allowed us to even overcome the requested noise level. Neptune, PKS 0537-441, and PKS 0402-362 were observed respectively as flux, bandpass, and phase calibrator. The data reduction was performed with CASA (version 3.4, McMullin et al. 2007; Petry & CASA Development Team 2012) in a standard way. Two antennas were flagged for bad system temperature and for phase drifts between two phase calibrator observations. The 4 spectral windows were calibrated separately and then averaged during the imaging using the MFS mode (Rau & Cornwell 2011). Flux densities were bootstrapped to the Neptune model and subsequently rescaled according to the more recent ‘Butler-JPL-Horizon 2012’<sup>1</sup> available in CASA from version 4.0 on.

The synthesized beam FWHM of  $0.84 \times 0.71$  arcsec is not small enough to image the star forming region details. However, since the source is detected with a high signal to noise ratio, it is possible to perform an analysis of visibilities in Fourier space and estimate the source size on scales smaller than that of the synthesized beam. By using the ‘uvmodelfit’ task provided with the CASA environment, we fitted the frequency-averaged visibilities with a single Gaussian component with a FWHM of  $0.27 \pm 0.08$  arcsec. This  $\sim 3.4\sigma$  indication of source extension has been cross checked with the package ‘mapping’ in the Gildas environment, which provided similar results. We note, however, that this measurement needs to be confirmed by data at even higher resolution, since at our longest baselines the sampling of the uv plane is sparse and the flux measurement could

<sup>1</sup> Buttel et al. 2012 [https://science.nrao.edu/facilities/alma/aboutALMA/Technology/ALMA\\_Memo\\_Series/alma594/abs594](https://science.nrao.edu/facilities/alma/aboutALMA/Technology/ALMA_Memo_Series/alma594/abs594)

**Table 1.** Summary of far-IR photometric datapoints

$\lambda_{obs}$ ( $\mu\text{m}$ )	$\lambda_{rest}$ ( $\mu\text{m}$ )	$S_\nu$ (mJy)	Beam (arcsec <sup>2</sup> )	Observatory	Refs
70	12	$< 0.9^a$	$6.5 \times 6.5$	Herschel/PACS	1
100	17	$< 0.6^a$	$7.4 \times 7.4$	Herschel/PACS	1
160	28	$< 1.3^a$	$11.3 \times 11.3$	Herschel/PACS	1
250	43	$4.1 \pm 1.9$	$18 \times 17$	Herschel/SPIRE	2
350	61	$< 12^a$	$25 \times 23$	Herschel/SPIRE	3
500	87	$< 15^a$	$37 \times 33$	Herschel/SPIRE	3
872	152	$6.1 \pm 0.5$	$2.1 \times 1.1$	ALMA band7	4
1181	205	$3.5 \pm 0.1$	$1.7 \times 1.5$	ALMA band6	5
1305	227	$2.47 \pm 0.07$	$0.84 \times 0.71$	ALMA band6	6
7500	1304	$< 0.04^a$	$12 \times 9$	ATCA	7

Notes: <sup>a</sup> $3\sigma$  upper limit. References: 1) Magnelli et al. (2013); 2) Daddi et al. in preparation; 3) Magnelli et al. (2012); 4) Hodge et al. (2013); 5) Nagao et al. (2012); 6) this work; 7) Coppin et al. (2010).

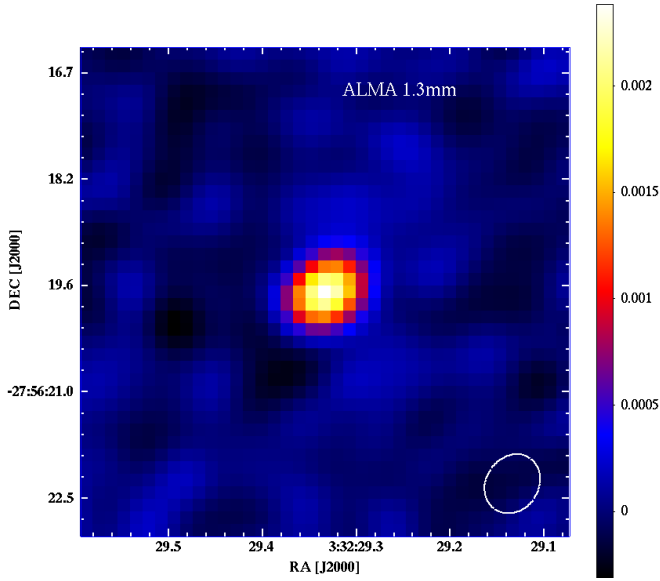


**Fig. 1.** ALMA intensity map of the 1.3mm dust continuum emission of XID403. The  $1\sigma$  rms is 0.07 mJy/beam. Units of the colorbar are Jy/beam. The cutout is  $6.5 \times 6.5$  arcsec, and the beam size is shown as a white ellipse ( $0.84 \times 0.71$  arcsec FWHM) on the bottom right. The source is unresolved, implying a half light radius of  $r_{half} < 2.5$  kpc.

be decreased by phase noise. The rms achieved in our image at 1.305mm is 0.07 mJy, and we measured a flux density at the peak of  $S_{1305} = 2.47$  mJy. The ALMA Band 6 image is shown in Fig. 1.

### 3. Far-IR SED: dust mass and temperature

Besides our data, there are two more continuum observations performed with ALMA on this source. The first was obtained by Nagao et al. (2012) at poorer resolution as a byproduct of their investigation of source metallicity through the [N II]205 $\mu\text{m}$  line: they measured a continuum flux density at  $\sim 1.2$  mm of  $S_{1181} = 3.5 \pm 0.1$  mJy. The other measurement was performed by Hodge et al. (2013) within a band 7 survey of the SMGs detected by LABOCA in the E-CDFS (XID403 is their ALESS 73.1): they measured  $S_{872} = 6.1 \pm 0.5$  mJy. These values are in excellent agreement with the flux densities derived from the  $5\sigma$  detections by AzTEC and LABOCA at 1.1mm and 870 $\mu\text{m}$ , respectively. At shorter wavelengths, faint emission can be seen at the posi-

tion of XID403 in the Herschel/SPIRE map at 250 $\mu\text{m}$ , for which a flux measurement was derived (at  $\sim 2\sigma$ ; Daddi et al. in preparation). Only upper limits to the source flux are available from the Herschel/PACS data (70, 100, 160 $\mu\text{m}$ ) or Herschel/SPIRE data at 350 and 500 $\mu\text{m}$  (Magnelli et al. 2012). For PACS observations, we used the  $3\sigma$  limits available for the deepest part of the PEP-GOODS-Herschel combined map Magnelli et al. (2013). Looser limits would be more appropriate at the position of XID403, but they would not have any impact on the derived best-fit SED (see below). For observations at 350 $\mu\text{m}$  and 500 $\mu\text{m}$ , we simply considered the  $3\sigma$  flux upper limits as derived in the SPIRE 24 $\mu\text{m}$ -prior catalogs ( $3\sigma$  confusion limits are slightly above these values (Magnelli et al. 2012). Recently, Swinbank et al. (2013) produced fully deblended SPIRE photometry of ALMA sources in the E-CDFS, deriving  $3\sigma$  limits of  $\sim 7$ ,  $\sim 8$ , and  $\sim 10$  mJy for XID403 (see their Fig. 4), which are consistent with the numbers we quote in Table 1 and with our best-fit SED (see below). An upper limit to the continuum flux at longer wavelengths ( $\sim 7.5$ mm) is also available from ATCA observations (Coppin et al. 2010). A summary of the available far-IR data is shown in Table 1.

We fit these data with a general modified blackbody model of the form (Rangwala et al. 2011):

$$S_{\nu_{obs}} \propto B_\nu(T)(1 - e^{-\tau_\nu}), \quad (1)$$

where

$$\tau_\nu = \left(\frac{\nu}{\nu_0}\right)^\beta \quad \text{and} \quad B_\nu(T) = \frac{2h\nu^3}{c^2} \frac{1}{e^{\frac{h\nu}{kT}} - 1}. \quad (2)$$

In the above equations  $\nu_{obs}$  and  $\nu$  are the observed and rest frequency, respectively [ $\nu = \nu_{obs}(1+z)$ ],  $\tau_\nu$  is the dust optical depth, and  $B_\nu(T)$  is the Planck function. Because of the limited number of photometric datapoints, we fixed the dust emissivity index to  $\beta = 2$  and the rest-wavelength at which the dust becomes optically thick (i.e.  $\tau_\nu = 1$ ) to  $\lambda_0 = c/\nu_0 = 200\mu\text{m}$  (i.e.  $\nu_0 = 1.5$  THz). These are consistent with the best fit values observed in distant SMGs with densely sampled SEDs (Conley et al. 2011; Fu et al. 2012; Riechers et al. 2013) and with what has been observed in the local ULIRG Arp220 (Rangwala et al. 2011). We note that most of the FIR datapoints available for XID403 are at  $\lambda_{rest} \lesssim 200\mu\text{m}$ , where the dust is likely optically thick. Therefore, the optically-thin grey-body approximation  $S_{\nu_{obs}} \propto B_\nu \tau_\nu$ , which is often used in the literature to fit FIR SEDs, cannot be utilized in this case, since it would severely underestimate the dust temperature (see e.g. Conley et al. 2011; Fu et al. 2012). A simple  $\chi^2$  fit to the FIR SED of XID403 returns an acceptable statistics with a best fit temperature of  $T_d = 58.5 \pm 5.3$ K (see Fig. 2), which is similar to what is measured with the same grey-body model in Arp220 ( $66.7 \pm 0.3$ K) and in high- $z$  SMGs with accurate SED determination. Once the best fit temperature and model normalization have been found, we determined the dust mass which is responsible for the total FIR emission by considering the model flux density at 1.3mm, where the dust is optically thin ( $\lambda_{rest} = 227\mu\text{m} > \lambda_0$ ) and the residual wrt to the ALMA data is minimal. We then used the standard relation valid for the optically thin case (e.g. Coppin et al. 2010; Greve et al. 2012):

$$M_d = \frac{D_L^2 S_{\nu_{obs}}}{(1+z)\kappa_\nu B_\nu(T_d)}, \quad (3)$$

where  $S_{\nu_{obs}}$  is the observed flux density at 1.3mm and  $\kappa_\nu$  and  $B_\nu(T_d)$  are computed at  $\nu = \nu_{obs}(1+z)$ . We adopt  $\kappa_\nu =$

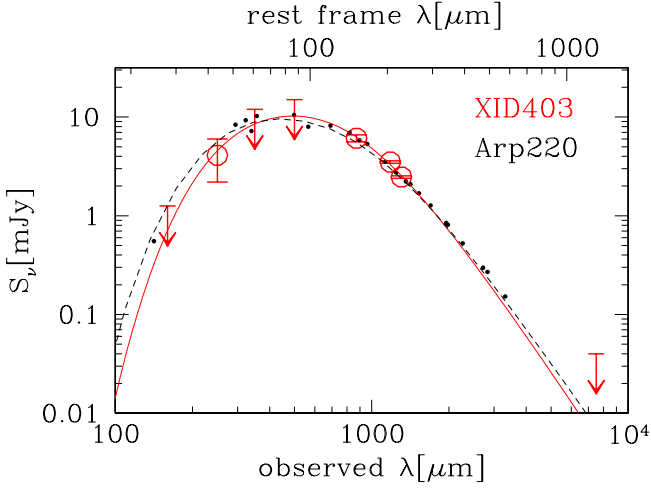


**Fig. 2.** Far-IR spectral energy distribution (SED) of XID403 (big red symbols and solid line) compared to that of the local starburst galaxy Arp220 (small black dots and dashed line; Rangwala et al. 2011) shifted to  $z=4.75$  and renormalized. The far-IR photometry of XID403 is reported in Table 1. The far-IR SED was fitted with a general modified black-body by fixing the emissivity index to  $\beta = 2$  and the rest-wavelength below which the dust is optically thick to  $\lambda_0 = 200\mu\text{m}$ , as commonly observed in high- $z$  SMGs (Conley et al. 2011; Fu et al. 2012; Riechers et al. 2013) and also in Arp220. The best-fit temperature is  $T_d = 58.5 \pm 5.3\text{K}$ . The best-fit dust mass is  $M_d = 4.9 \pm 0.7 \times 10^8 M_\odot$  (see text for details).

$4.0(\nu/1.2\text{THz})^\beta \text{cm}^2 \text{g}^{-1}$  with  $\beta = 2.0$ . These prescriptions for the absorption cross section  $\kappa_\nu$  and the emissivity index  $\beta$  are consistent with those derived from full dust models which consider a distribution of dust grains and a range of interstellar radiation field densities (e.g. Draine & Li 2007). The dust masses determined with Eq.3 using these prescriptions are in excellent agreement with those determined by full dust models (Bianchi 2013). For XID403 we measured  $M_d = 4.9 \pm 0.7 \times 10^8 M_\odot$ . The large dust content of this object is comparable to the ones derived in starbursting QSO hosts at similar or even higher redshifts (Wang et al. 2013a; Calura et al. 2013).

#### 4. Star formation rate and compactness

By integrating the best-fit modified greybody spectrum we obtained a far-IR (42.5-122.5 $\mu\text{m}$ ) luminosity of  $L_{\text{FIR}} = 4.2 \pm 0.6 \times 10^{12} L_\odot$  and a total-IR (8-1000 $\mu\text{m}$ ) luminosity of  $L_{\text{IR}} = 5.9 \pm 0.9 \times 10^{12} L_\odot$ , where the 15% quoted uncertainties just take into account the statistical uncertainties on the greybody model normalization. These values are in excellent agreement with those previously derived by Coppin et al. (2009) and Gilli et al. (2011) and have significantly smaller uncertainties. By using the Kennicutt (1998) relation  $\text{SFR}(M_\odot/\text{yr}) = 1.74 \times 10^{-10} L_{\text{IR}}(L_\odot)$  we derived a star formation rate of  $\text{SFR} = 1020 \pm 150 M_\odot \text{yr}^{-1}$ . We note that this value has been obtained by the integration of the single greybody component, and therefore is not contaminated by AGN emission, which instead contributes significantly to the *total* SED at  $\lambda_{\text{rest}} \lesssim 20\mu\text{m}$  (see Gilli et al. 2011 and Fig. 3). Based on the ALMA image at 1.3mm, where the source emission is spatially unresolved on sub-arcsec scales, (beam FWHM $\sim 0.75$  arcsec) we can derive an upper limit of  $r_{\text{half}} < 2.5\text{kpc}$  to the half-light radius of the dust continuum

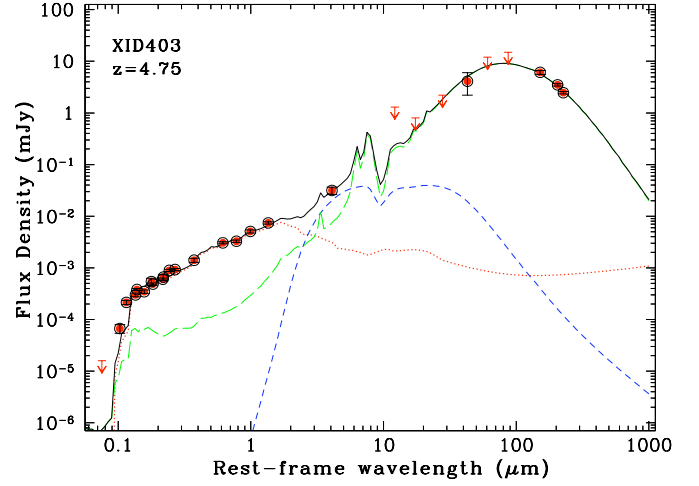


**Fig. 3.** Rest-frame SED of XID403 and its spectral decomposition. Photometric datapoints and  $3\sigma$  upper limits are marked by red filled points and downward-pointing arrows, respectively. The total SED (black solid line) is the summed contribution of the stellar (red dotted line), AGN (blue short-dashed line), and star-forming (green long-dashed line) components. See text for details.

emission ( $r_{\text{half}} = 0.9 \pm 0.3 \text{kpc}$  based on the analysis of visibilities)<sup>2</sup>. The observed star formation hence is produced within a kpc-scale region, and a lower limit to the rate of star formation per unit area  $\Sigma_{\text{SFR}} = (\text{SFR}/2)/(\pi r_{\text{half}}^2) > 26 M_\odot \text{yr}^{-1} \text{kpc}^{-2}$  can be obtained ( $\Sigma_{\text{SFR}} = 200 M_\odot \text{yr}^{-1} \text{kpc}^{-2}$  for  $r_{\text{half}} = 0.9 \text{kpc}$ ). Highly-starforming galaxies (LIRGs/ULIRGs) both in the local and distant Universe are usually making their stars in compact bursts with  $\Sigma_{\text{SFR}} \sim 10 - 100 M_\odot \text{yr}^{-1} \text{kpc}^{-2}$  (see e.g. Genzel et al. 2010 and references therein). Hodge et al. (2013) derived a median SFR surface density of  $> 14 M_\odot \text{yr}^{-1} \text{kpc}^{-2}$  for their sample of SMGs observed by ALMA in the ECDFS at median  $z \sim 2.2$ . The value we measured for XID403 is in line with these findings.

#### 5. SED decomposition

The CDFS features the deepest multiwavelength database available in a given patch of the sky. Very recently the CANDELS GOODS-South catalog has been released (Guo et al. 2013) which provides optical to near-IR photometry information for about 35,000 H-band detected sources (HST/WFC3 F160W band) in the GOODS portion of the CDFS. XID403 is detected at 1.6 $\mu\text{m}$  with a flux of  $0.926 \pm 0.023 \mu\text{Jy}$  (23.89 AB mag). We retrieved all the photometry available for XID403 from the CANDELS catalog, including HST optical/near-IR imaging with ACS and WFC3 (from 0.4 to 1.6  $\mu\text{m}$ ), VLT K-band imaging (HAWK-I and ISAAC) and Spitzer/IRAC near-IR imaging (from 3.6 to 8.0  $\mu\text{m}$ ). We added to those data Spitzer/MIPS photometry at 24 $\mu\text{m}$  and the FIR data from Herschel and ALMA described in the previous Sections. A complete and extremely well sampled SED is then obtained, which is shown in Fig. 3.

The optical to far-infrared (millimeter) data of XID403 were modelled using the spectral energy distribution (SED) fitting code originally developed by Fritz et al. (2006) and recently updated by Feltre et al. (2013). This code allows the user to

<sup>2</sup> One arcsec is 6.6kpc at  $z = 4.75$ ; we also recall that, for a Gaussian beam,  $r_{\text{half}} = \text{FWHM}/2$ .

fit broad-band data using three components: i) a stellar component for the host galaxy, whose contribution is dominant in the optical/near-IR bands; ii) an AGN component due to nuclear emission (mostly UV) reprocessed by hot dust, peaking at a few tens of microns; iii) a star-forming component, which accounts for the far-IR blackbody-like thermal bump (see Pozzi et al. 2010, 2012 and Vignali et al. 2009, 2011 for recent applications of this code).

The stellar component (red dotted line in Fig. 3) comprises a set of simple stellar population (SSP) spectra of solar metallicity and ages up to 0.6 Gyr, i.e., the time elapsed between  $z_{\text{form}}=8$  (the redshift here assumed for the stars to form) and  $z = 4.75$  (the source redshift). Extinction to the stellar component is modelled using a Calzetti et al. (2000) attenuation law.

We modeled the AGN component (blue short-dashed line in Fig. 3) using a smooth torus model with a “flared disc” geometry (see Fritz et al. 2006). Although high-resolution mid-IR observations of nearby AGN have suggested that a clumpy configuration for the obscuring torus is probably more likely (e.g., Jaffe et al. 2004; Tristram et al. 2007; Burtscher et al. 2013), smooth and clumpy torus models provide equally good descriptions of the AGN infrared SEDs (as extensively discussed by Feltre et al. 2012).

Finally, the far-IR emission has been reproduced using dusty SSPs (comparably good results are obtained using empirical starburst FIR templates). The SSP fit is shown as a long-dashed line in Fig. 3). These dusty SSPs share the same star formation history of those used to fit the optical-UV part of the spectrum: their emission appears strongly extinguished in the optical (see Fig. 3), but they are able to reproduce the whole far-IR thermal bump.

Overall, the SED fitting to the available datapoints is extremely good (black solid line in Fig. 3) and allows us to estimate many of the relevant physical parameters of both the host galaxy (e.g. stellar mass, optical extinction, SFR) and the AGN (e.g. bolometric luminosity). The large amount of information at optical/near-IR wavelengths provides a reliable estimate of the stellar mass  $M_* \sim 1.1 \times 10^{11} M_{\odot}$  (the average value measured for ALESS SMGs is  $8 \pm 1 \times 10^{10} M_{\odot}$ ; Simpson et al. 2013), where the estimated uncertainties on  $M_*$  are within 50% and are dominated by systematics, e.g. by the choice of the IMF (we used a Salpeter IMF). Significant extinction to the host galaxy emission is also required [ $E(B-V)=0.33$ ]. For what concerns the AGN, its contribution mostly relies on the *Spitzer*/MIPS photometric datapoint at  $24\mu\text{m}$  (see also Coppin et al. 2009). This does not allow us to constrain the geometric AGN parameters (e.g., the opening angle of the torus). However, the source bolometric accretion luminosity appears to be well determined to  $\sim 10^{46} \text{ erg s}^{-1}$  ( $2.6 \times 10^{12} L_{\odot}$ ). This value is in excellent agreement with what is derived from the 2-10 keV intrinsic luminosity assuming appropriate bolometric corrections (Lusso et al. 2012) and is about half of the total luminosity produced by stellar processes ( $L_{\text{IR}} = 5.9 \times 10^{12} L_{\odot}$ ).

As evident in Fig. 3, the AGN contributes 2–3% of the 8–1000 $\mu\text{m}$  emission. Once corrected for this contribution, the far-IR luminosity can be used to derive a star-formation rate of  $\sim 1040 M_{\odot}/\text{yr}$ , in excellent agreement with what has been estimated in Section 4. This value is much larger than the one obtained by fitting the optical/near-IR SED ( $\sim 290 M_{\odot}/\text{yr}$ ). As discussed in Section 7.2, such a discrepancy is often found when fitting the broad band SEDs of LIRGs/ULIRGs and can be explained, at least to zeroth order, in terms of most star-formation occurring in heavily obscured, dust-embedded environments (as also assumed in dusty SSP models; da Cunha et al. 2008).

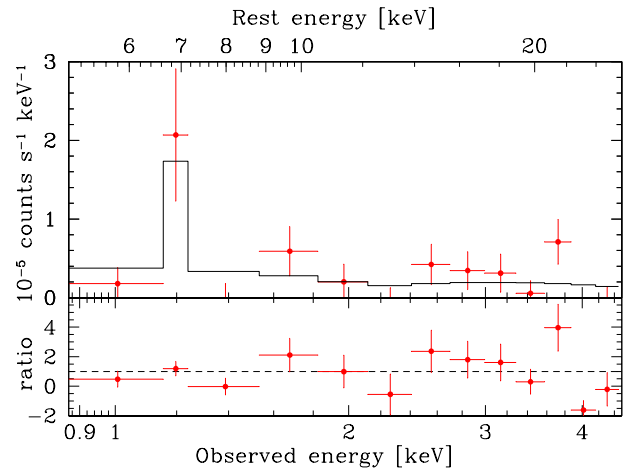


**Fig. 4.** 4Ms Chandra X-ray spectrum of XID403 and ratio to the best fit model (see text for details). A Fe emission line at  $\sim 6.9$  keV rest-frame is detected at  $\sim 2\sigma$ .

## 6. X-ray emission: photons from highly-ionized iron?

As reported by Gilli et al. (2011), the hard X-ray spectrum of XID403 strongly points to heavy, Compton-thick absorption. The best-fit absorption column density was found to be  $1.4^{+0.9}_{-0.5} \times 10^{24} \text{ cm}^{-2}$ . Similar values were derived by Vito et al. (2013;  $1.8^{+1.5}_{-0.8} \times 10^{24} \text{ cm}^{-2}$ ) and Wang et al. (2013b;  $\approx 0.8 \times 10^{24} \text{ cm}^{-2}$ ). However, even higher columns could not be ruled out. Indeed, when  $N_H \gtrsim 10^{25} \text{ cm}^{-2}$ , the direct X-ray nuclear radiation is completely blocked, and only photons scattered by matter off the line of sight can be detected. In the case of XID403, a simple Compton reflection continuum from cold gas surrounding the nucleus provided an equally good fit to the X-ray spectrum. In Gilli et al. (2011) we did not detect any iron emission line at 6.4 keV rest-frame. This prominent line (equivalent width  $\text{EW} \sim 1 - 2 \text{ keV}$ ) is commonly observed in Compton-thick AGN (e.g. Comastri 2004) and usually interpreted as a fluorescence line associated to low-ionized iron atoms (up to Fe xvii) in the cold reflector. The upper limit we could place on the line EW, however, was very loose ( $\text{EW} < 4.3 \text{ keV}$  at 90% confidence level) and did not contrast with the interpretation of a heavily obscured nucleus. Here we have re-analyzed the 4Ms Chandra X-ray spectrum of XID403 and performed a more detailed search of iron emission features. In particular, we were prompted by the results of Iwasawa et al. (2012), who found evidence of high-ionization lines from Fe xxv at 6.70 keV and Fe xxvi at 6.97 keV in the stacked spectrum of 33 obscured AGN hosted by ULIRGs in the COSMOS field. The details of the data reduction and X-ray spectral analysis of XID403 are presented in Gilli et al. (2011). We now fit that spectrum with a pure reflection continuum (pexrav model in XSPEC) plus an iron line at a centroid energy which is left free to vary. We used the Cash statistic to estimate the best fit parameters. Errors are quoted at  $1\sigma$  confidence level ( $\Delta C = 1$ ). We found a  $\sim 2\sigma$  evidence for a line at  $\sim 1.19 \text{ keV}$ , i.e.  $\sim 6.9 \text{ keV}$  rest-energy ( $6.88 \pm 0.16 \text{ keV}$ ; see Fig.4), which can be interpreted as emission from highly ionized iron. The same feature is confirmed when we consider the Chandra spectrum obtained by Vito et al. (2013) who performed a completely independent spectral extraction and background subtraction. As a safety check, we verified that no significant emission

**Table 2.** Summary of the physical properties of XID403

Quantity	Value	Units	Reference
$L_{FIR}$	$4.2 \pm 0.6$	$10^{12} L_{\odot}$	this work
$L_{IR}$	$5.9 \pm 0.9$	$10^{12} L_{\odot}$	this work
$L_{AGN}^{bol}$	2.6	$10^{12} L_{\odot}$	this work
SFR	$1020 \pm 150$	$M_{\odot} \text{yr}^{-1}$	this work
$M_{dust}$	$4.9 \pm 0.7$	$10^8 M_{\odot}$	this work
$T_{dust}$	$58.5 \pm 5.3$	K	this work
$r_{half}$	$< 2.5$	kpc	this work
$\Sigma_{SFR}$	$> 26$	$M_{\odot} \text{yr}^{-1} \text{kpc}^{-2}$	this work
$M_{HI}$	$1.0 \pm 0.3$	$10^{10} M_{\odot}$	De Breuck et al. (2011)
$M_{H_2}$	$1.6 \pm 0.3$	$10^{10} M_{\odot}$	Coppin et al. (2010)
$\Sigma_{H1+H2}$	$> 6.6$	$10^8 M_{\odot} \text{kpc}^{-2}$	this work
$N_{H1+H2}$	$> 0.1$	$10^{24} \text{cm}^{-2}$	this work
$N_H^{X\text{-ray}}$	$1.4^{+0.9}_{-0.5}$	$10^{24} \text{cm}^{-2}$	Gilli et al. (2011)
$M_{dyn} \sin^2 i$	$1.2 \pm 0.6$	$10^{10} M_{\odot}$	Coppin et al. (2010)
$M_*$	11	$10^{10} M_{\odot}$	this work
$Z$	$1.0^{+1.0}_{-0.6}$	$Z_{\odot}$	Nagao et al. (2012)

Notes: The dynamical mass estimated by Coppin et al. (2010) assumes a disk-like geometry where  $i$  is the inclination angle of the disk axis to the line of sight.

features at that energy are present in the Chandra background spectrum. The rest-frame line EW is  $2.8^{+1.7}_{-1.4}$  keV: indeed, given the low S/N of the spectrum and the redshift dimming of the observed equivalent width [ $EW_{obs} = EW_{rest}/(1+z)$ ], only extreme features can be detected with some confidence. The measured EW is very large for what is commonly seen in X-ray spectra but not unreasonable (see Matt et al. 1996 for a theoretical perspective). In particular, there is mounting evidence that ULIRGs and SMGs both in the local and distant Universe feature He-like and H-like Fe lines at 6.7 and 6.9 keV with large,  $\sim 1 - 2$  keV, equivalent widths (e.g. Iwasawa et al. 2009; Lindner et al. 2012). In particular, such lines with EW up to  $\sim 2$  keV have been detected in powerful starforming objects hosting heavily obscured AGN (Iwasawa et al. 2005; Nandra & Iwasawa 2007; Nardini & Risaliti 2011; Jia et al. 2012). The tentative detection in XID403 of an emission feature from highly-ionized iron would be in line with these findings. We will return on the Fe line detection and its interpretation in the Discussion.

## 7. Discussion

### 7.1. Size of the system

The sub-arcsec ALMA observations reported in this work constrain the FIR dust continuum to be emitted within a half-light radius of  $r_{half} < 2.5$  kpc from the central SMBH (and also suggest at the  $\sim 3\sigma$  level that  $r_{half}$  could be around 0.9 kpc). Observations of high- $z$  QSOs (Wang et al. 2013a) show that both CO and [CII] emission are co-spatial with FIR emission. Furthermore, Riechers et al. (2011) showed that, as opposed to high- $z$  SMGs, high- $z$  QSOs do not show evidence of extended, low-excitation molecular gas components. Then, under the reasonable assumption that both molecular and atomic gas are co-spatial with dust also in XID403, we obtain that, if half of the total gas mass  $M_{gas} = M_{H_2} + M_{HI} = 2.6 \times 10^{10} M_{\odot}$  (Coppin et al. 2010; De Breuck et al. 2011) is confined within 2.5 kpc from the nucleus, this would produce a column density of  $N_H > 0.1 \times 10^{24} \text{cm}^{-2}$  towards it.<sup>3</sup> For  $r_{half} = 0.9 \pm 0.3$  kpc,

<sup>3</sup> Based on a recent estimate from ALMA data (De Breuck et al. priv. comm.), the [CII] luminosity and hence  $M_{HI}$  derived in De Breuck et al. (2011) are likely overestimated by a factor of  $\sim 2$ . This would decrease

we estimate  $N_H = 0.3 - 1.1 \times 10^{24} \text{cm}^{-2}$ , which is consistent with what is inferred from the X-ray spectrum and shows that, in principle, absorption on galaxy scales could be sufficient to hide the nucleus without invoking any additional pc-scale obscuring matter (the estimated column density would instead be overestimated if the gas reservoir is more extended than dust; see e.g. Swinbank et al. 2012 and references therein). Recent numerical simulations indeed show that high redshift galaxies hosting dense and thick disks of gas on kpc scales may provide heavy absorption (up to Compton-thick) towards their central black hole (Bournaud et al. 2011), and a physical link between nuclear absorption and host gas content has been suggested even for AGN at  $z < 1$  (Juneau et al. 2013). We note that the column density derived from the X-ray spectrum was obtained assuming a solar metallicity for the obscuring medium. This is consistent with what has been measured by Nagao et al. (2012) for the metallicity of the gas in the circumnuclear starburst. Nevertheless, we cannot rule out the presence of a compact inner absorber around the nucleus. The presence of a dense medium on pc scales from the nucleus is indeed revealed by the presence of hot, AGN-heated dust at  $4\mu\text{m}$  rest-frame (see Fig. 3). However, since both the covering factor and the inclination along the line of sight of this compact medium cannot be constrained, it is not clear how much of the nuclear obscuration it produces.

The HST observations in the UV/optical rest-frame can be used to get another estimate of the size of the system, although it is likely that UV light is not tracing the entire dimensions of the system as most star formation is occurring in dust-obscured regions (see Section 5). The emission in the HST/ACS z-band is unresolved at 0.1 arcsec resolution (FWHM), pointing to a half-light radius of stellar emission of  $< 0.3$  kpc at  $\sim 1600\text{\AA}$  rest-frame (Coppin et al. 2009; Gilli et al. 2011). In the HST/WFC3 H-band, the source is detected with a stellarity parameter of 0.9 (Guo et al. 2013). That is, the source could be marginally resolved at a resolution of 0.3 arcsec at  $\sim 2800\text{\AA}$  rest-frame, which would give a half-light radius of  $\sim 1$  kpc for stellar emission, similar to what is found for dust emission. Any contribution of the AGN to the optical/UV emission, e.g. through scattered light, cannot be quantified precisely. However, as opposed to Gilli et al. (2011), we suggest here that most of the optical/UV light is produced by stars. First, the broad band SED obtained from the CANDELS catalog seems very smooth and a simple galaxy template provides an excellent fit without requiring any additional component (see Fig. 3). Second, extremely compact morphologies with half-light radii as small as  $\sim 0.1$  kpc have been recently observed in highly star forming systems without AGN that reach star formation rate densities of  $\sim 3000 M_{\odot} \text{yr}^{-1} \text{kpc}^{-2}$  (Diamond-Stanic et al. 2012). Third, the rest-frame UV spectrum of XID403 closely resembles those of local compact starbursts (see Section 7.4). We have therefore some indications that, if both stars, gas and dust were co-spatial, the system size could realistically be  $\sim 0.9$  kpc and as small as 0.3 kpc.

### 7.2. Dusty Star Formation

If the entire FIR emission in XID403 is interpreted as thermal emission from dust heated by young stars using the calibration derived by Kennicutt (1998), then a SFR of  $\sim 1000 M_{\odot} \text{yr}^{-1}$  is derived. Such a large rate is not observed in the local Universe, but is frequently observed in high redshift galaxies (e.g. Magnelli et al. 2012). In the most luminous IR systems, the

all our estimates of total gas densities by  $\sim 20\%$ , without affecting significantly our results

SFR derived from the FIR emission is usually larger than what is derived by the UV stellar light (e.g. Bongiorno et al. 2012; Casey et al. 2013). This is the case also for XID403, where the UV-estimated SFR, even after correcting for optical reddening, is a factor of  $\sim 3$  lower than that estimated from the IR. A plausible interpretation for this difference is that, in luminous IR systems, most stars form in very dusty regions and hence do not produce any light that can contribute to the optical SED. Recently, Lo Faro et al. (2013) suggested that the majority of the IR emission in LIRGs and ULIRGs (at  $z \sim 1 - 2$ ) is produced by diffuse dust (“cirrus”) heated by intermediate-age ( $10^8 - 10^9$ yr) rather than by young ( $< 10^8$ yr) stellar populations. This would lead to an overestimate of the IR-derived SFRs by a factor of 2-3, while those derived from the UV-light would be more reliable indicators. However, for extreme star formation rates, such as that measured in XID403, the emission of dust heated by intermediate-age stars is expected to be small, and the total FIR emission appears to be a good proxy of the global SFR (see Lo Faro et al. 2013 for details).

By fitting the FIR SED with a modified blackbody we find that the dust is warm,  $T_d = 58.5 \pm 5.3$  K. Warm dust appears to be typical of ULIRGs both in the local (e.g. Arp220, Rangwala et al. 2011) and in the distant Universe (Fu et al. 2012; Riechers et al. 2013). This temperature has been derived by adopting a general grey body emission, i.e. we did not assume that dust is optically thin. Should we adopt the optically-thin greybody approximation, as often done in the literature, we would measure a colder dust temperature  $T_d \sim 33$  K. This is because of the stronger emission at shortest wavelengths in the optically thin approximation (see Eqs. 1 and 2), which therefore needs a cooler temperature to fit an SED bump at a fixed wavelength. This has been already discussed in the literature (Conley et al. 2011; Fu et al. 2012). We note here that the temperature derived for XID403 in the optically-thin approximation is of the same order of that observed in ULIRGs and SMGs when using the same approximation (Casey 2012). That is, the FIR peak emission of XID403 again seems in line with what has been observed in intense starburst systems.

A different parameterization to the FIR SED on SMGs in the ALMA-LABOCA survey of the ECDFS (ALESS) has been adopted by Swinbank et al. (2013). They used three dust components (cold,  $T = 20 - 30$  K; warm,  $T = 50 - 60$  K; and hot,  $T = 80 - 120$  K) and allowed the dust emissivity index to vary within  $\beta = 1.5 - 2.0$  to derive mass and temperature of the various components: the cold and warm components are those contributing to the peak SED emission, with the cold component dominating the total mass budget of the dust. Although the different parameterizations prevent a straightforward comparison between our results and those by Swinbank et al. (2013), we note that the dust mass we derived is in line with their average value of  $\sim 4 \times 10^8 M_\odot$ . The  $L_{IR}$  and SFR we measured for XID403 are also comparable to those of high- $z$  sources in the ALESS sample.

Magdis et al. (2012) studied the decrease of the gas-to-dust mass ratio with metallicity for a few samples of “main-sequence” and starburst galaxies both in the local and distant Universe: starburst systems tend to have higher metallicities and lower gas-to-dust mass ratios than main-sequence star forming galaxies. They then used the observed  $M_{gas}/M_{dust} \propto 1/Z$  relation as a proxy to determine the molecular gas mass  $M_{H_2}$  in their systems ( $M_{gas} = M_{HI} + M_{H_2}$ , so if both  $M_{HI}$ ,  $M_{dust}$ , and  $Z$  are known,  $M_{H_2}$  can be derived) and finally estimate the conversion factor  $\alpha_{CO}$  between CO luminosity  $L'_{CO}$  and molecular gas mass ( $M_{H_2} = \alpha_{CO} L'_{CO}$ ). For local ULIRGs and distant

SMGs they found  $\alpha_{CO} \sim 1$ , which is consistent with the standard value of 0.8 assumed for starburst systems (Solomon & Vanden Bout 2005). For XID403 we measured a dust mass of  $M_d = 4.9 \pm 0.8 \times 10^8 M_\odot$ . This, when compared with the total (atomic + molecular) gas mass estimated from previous works (see Table 2), translates into a gas-to-dust mass ratio of  $\sim 50$  for a medium with solar metallicities (Nagao et al. 2012), and places XID403 in the region populated by local and distant starburst galaxies. The molecular gas mass derived using the relation by Magdis et al. (2012) is  $M_{H_2} \sim 3.2 \times 10^{10} M_\odot$ , suggesting that a conversion factor of the order of 0.8-1 also applies to XID403 (Coppin et al. 2010 indeed used  $\alpha_{CO} = 0.8$  to derive  $M_{H_2} = 2.6 \times 10^{10} M_\odot$ ).

Our ALMA observations have placed a lower limit of  $26 M_\odot \text{yr}^{-1} \text{kpc}^{-2}$  to the star formation rate density in XID403. Assuming that both atomic and molecular gas are co-spatial with the dust probed by ALMA observations, we can similarly estimate a gas surface density of  $\Sigma_{gas} = \Sigma_{HI+H_2} = (M_{HI+H_2}/2)/(\pi r_{half}^2) > 6.6 \times 10^8 M_\odot \text{kpc}^{-2}$  (see Table 2). These values place XID403 above the sequence of star forming galaxies following the Schmidt-Kennicutt law (Schmidt 1959; Kennicutt 1998) that relates the surface density of star formation with that of gas observed in both local and distant disk galaxies (Daddi et al. 2010). Instead, XID403 falls within the sequence of starburst galaxies at  $z = 0 - 2$  of Daddi et al. (2010), which are forming stars at a rate ten times higher than that of disk galaxies for a given gas density.

### 7.3. Physics of the system and blow-out condition

The high star formation density measured in XID403 is in line with the values measured in many distant star forming galaxies, which can even reach values as high as  $\sim 3000 M_\odot \text{yr}^{-1} \text{kpc}^{-2}$  (Diamond-Stanic et al. 2012; Geach et al. 2013; Riechers et al. 2013). A ubiquitous feature of star forming galaxies both in the local and distant Universe is that they undergo significant mass outflows (Bordoloi et al. 2013), with the outflow rate being proportional to the star formation rate density. In the extreme systems described by Diamond-Stanic et al. (2012), outflow velocities of  $\geq 1000$  km/s have been measured.

It is then instructive to estimate the physical conditions in XID403 and provide an order of magnitude estimate about the likelihood that a large scale outflow is launched. Assuming that a fraction  $\epsilon$  of the available gas in the system is converted into stars (i.e.  $\epsilon$  is the star formation efficiency), one has that  $SFR = \epsilon f_{gas} M_{tot}/t_d$ , where  $M_{tot}$  is the total mass of the system,  $f_{gas}$  is the gas fraction and  $t_d$  is the dynamical time. By considering that the system velocity dispersion is  $\sigma_{tot} \sim (GM_{tot}/R)^{1/2}$ , where  $R$  is the size of the system, and that  $t_d \sim (G\rho_{tot})^{-1/2}$ , where  $\rho_{tot}$  is the total mass density, one can write:  $SFR \sim \epsilon f_{gas} \sigma_{tot}^3/G$ . The turbulent pressure that is produced by star formation onto the ISM (either through SN feedback, stellar winds, H II region expansion, cosmic rays; Ostriker & Shetty 2011) is  $P_t = \rho_{gas} \sigma_{gas}^2$ , where  $\sigma_{gas}$  is the turbulent velocity dispersion of the gas. It has been shown (Förster Schreiber et al. 2009; Newman et al. 2013) that moving from the local Universe to  $z \sim 1 - 2$  the average gas velocity dispersion of star forming galaxies increases and is a strong function of the galaxy size. In particular, compact systems are more likely to be dispersion-dominated, with  $\sigma_{gas} \sim 70 - 80$  km/s for  $r_{half} < 1$  kpc at  $z \sim 1 - 2$ . By extrapolating this trend to  $z > 4$  (as also expected by models of galaxy growth, in which high-redshift systems are predominantly unstable, dispersion-dominated systems that later form extended rotationally sup-

ported disks; see Law et al. 2012 and references therein), we will then assume that in XID403 the gas velocity dispersion is even higher than that of similar-size systems at  $z \sim 1 - 2$ , and is of the same order of the total (stellar) velocity dispersion ( $\sigma_{gas} \approx \sigma_{tot}$ ). We can therefore write the turbulent pressure injected by star formation into the ISM as:  $P_t = \rho_{gas}[G SFR/(\epsilon f_{gas})]^{2/3}$ . The total vertical weight in a self-gravitating gas disk is  $P_{disk} = \pi G \Sigma_{gas}^2/2$ , where  $\Sigma_{gas}$  is the gas surface density (Ostriker & Shetty 2011). The conditions for a blow-out of the disk are met and a large-scale outflow is expected to occur when:

$$C \equiv P_t/P_{disk} = \frac{2}{\pi G^{1/3}} \frac{\rho_{gas}}{\Sigma_{gas}^2} \left( \frac{SFR}{\epsilon f_{gas}} \right)^{2/3} > 1. \quad (4)$$

To estimate  $\rho_{gas}$ , assuming the gas is distributed into a disk, its scale height needs to be known. The detailed morphology of XID403 is unknown. Starbursting systems at high redshift may have complex morphologies, possibly as a result of recent mergers (Schinnerer et al. 2008; Tacconi et al. 2008). However, disk-like morphologies of cold gas have been observed in a significant fraction of starforming galaxies hosting QSOs at epochs as early as  $z \sim 6$  (Wang et al. 2013a). By assuming a scale-height of the order of the disk size (i.e. a spherical volume), we can at least provide a lower limit to  $\rho_{gas}$ , an upper limit to  $\epsilon \propto t_d \propto \rho_{gas}^{-1/2}$ , and hence a conservative lower limit to  $C$ . Then, for  $r_{half} < 2.5$  kpc,  $\rho_{gas} > 1.3 \times 10^{-23}$  g cm $^{-3}$ ,  $\tau_d < 3.4 \times 10^7$  yr,  $\epsilon < 1$ . Finally, by considering  $f_{gas} = M_{gas}/(M_{gas} + M_*) \sim 0.2$  and substituting into Eq. 4, we obtain  $C > 5$ , suggesting that the blow-out condition is met and a large scale gas outflow should occur. Interestingly, this computed blow-out condition is scale-free. Indeed,  $C \propto \rho_{gas} \Sigma_{gas}^{-2} \tau_d^{-2/3} \propto r^{-3} r^4 r^{-1} \propto r^0$ . Therefore, the blow-out condition will be met also for a system size of  $r_{half} \sim 0.9$  kpc or smaller (note that this blow-out condition cannot be applied to large,  $\gg 2$  kpc, rotation-dominated systems).

#### 7.4. Possible evidence for outflowing gas

Based on the above considerations we searched for evidence of an outflow in XID403, and first considered its optical spectrum. Besides the observations performed at Keck (Coppin et al. 2009), the source was observed twice during the GOODS-FORS2 campaign (Vanzella et al. 2008). We improved the data reduction originally published in Vanzella et al. (2008) by including the more recent procedures adopted in Vanzella et al. (2011). The two FORS2 spectra were re-analyzed and stacked, providing a final spectrum of 6.3 hours integration time (see Fig. 5).

A first piece of evidence for outflowing gas could be the velocity shift observed between the Ly $\alpha$  emission and the submm lines of [NII], [CII], CO(2-1)<sup>4</sup> (see Fig. 2 in Nagao et al. 2012 and Fig. 5). If one assumes that e.g. the [NII] emission is tracing the systemic redshift, then Ly $\alpha$  is red-shifted by  $\sim 350$  km s $^{-1}$ . Redshifted Ly $\alpha$  emission by 100-1000 km s $^{-1}$  is commonly observed in Lyman Break Galaxies (Steidel et al. 2010), and is interpreted as evidence for outflowing gas: in this scenario the observed Ly $\alpha$  emission would arise from the receding side of the outflow, once the Ly $\alpha$  photons have been red-shifted by several hundreds km s $^{-1}$  relative to the bulk of the

material they have to cross to reach us (blue-shifted Ly $\alpha$  photons are instead efficiently absorbed within the system). This interpretation is however complicated by the fact that radiative transfer processes strongly shape the emerging Ly $\alpha$  line profile and peak wavelength, which in fact depend on the gas column density, dust mass and their unknown geometrical distribution. Moreover, at high redshift, the blue side of the Ly $\alpha$  emission can be also depressed by absorption in the neutral intergalactic medium (IGM). Besides Ly $\alpha$  emission, the optical spectrum of XID403 also shows a rather broad ( $\sim 2200$  km s $^{-1}$  FWHM) N v 1240 feature of comparable flux, which was regarded as the signature of an AGN (Vanzella et al. 2006; Coppin et al. 2009). One possible problem with the AGN interpretation is the width of the N v line, which should be produced by Broad Line Clouds at sub-pc scales from the black hole, and would suggest an unobscured view of the nucleus (unless one is seeing scattered radiation): such a direct-view scenario is probably unfavored by the large amount of obscuration measured in the X-rays and also by the large amount of gas and dust confined within a radius that could be as small as a few hundreds pc (see Section 7.2). Here we suggest that, instead, the broad N v 1240 could arise from stellar winds produced by hot (O) stars present in this massive starburst system. These winds would produce P-cygni profiles. Although, to our knowledge, no such features have been observed at high redshift, they have indeed been detected in starforming galaxies in the local Universe (Heckman et al. 2011; Leitherer et al. 2013). In particular, Heckman et al. (2011) present HST/COS UV spectra of a sample of ten Lyman Break Analogs, i.e. a rare population of local galaxies with UV luminosities and surface densities similar to high- $z$  Lyman Break Galaxies, where high velocity outflows have been detected ( $\sim 600$  km s $^{-1}$  median) in all of them and very compact starbursts ( $r \sim 0.1$  kpc) in about 40% of them. The UV spectra presented by Heckman et al. (2010), are strikingly similar to that of XID403, i.e. they also have Ly $\alpha$  peaks redshifted with respect to the systemic velocity and similar Ly $\alpha$  profiles, Ly $\alpha$ /N v ratios, N v widths. We also note that the profile of the N v line in XID403 may hint to a P-Cygni profile with a depression in the continuum blueward of N v (see Fig. 5). The detection of the stellar UV continuum and line emission is in agreement with the SED analysis (see Fig. 3). In extremely dusty systems, the detection of stellar UV light can be ascribed to an inhomogeneous ISM, as suggested for instance by the analysis of Leitherer et al. (2013) on four local UV-selected LIRGs. We therefore conclude that in XID403 there is reasonable evidence for strong stellar winds from hot and massive stars. Together with supernovae explosions (Murray et al. 2005) and AGN feedback (Maiolino et al. 2012) these winds are one of those mechanisms which would be able to launch galactic-scale outflows (Leitherer et al. 1992).

Another emission feature of XID403 which deserves some discussion is the line at  $\sim 6.9$  keV likely arising from Fe xxvi, for which a rest frame equivalent width of  $EW_{rest} = 2.8_{-1.4}^{+1.7}$  keV was measured. The line detection is admittedly uncertain ( $2\sigma$ ), but we note that prominent emission lines from highly-ionized iron have been found in many LIRGs and ULIRGs (with or without AGN) both in the local and distant Universe (Iwasawa et al. 2009; Lindner et al. 2012). Notable examples of such lines, with EW up to  $\sim 2$  keV, have been detected in powerful starforming objects which are known to contain heavily obscured AGN like Arp220 (Iwasawa et al. 2005), the Superantennae (Jia et al. 2012), IRAS 12127-1412 (Nardini & Risaliti 2011) or the HyLIRG IRAS 00182-7112 (Nandra & Iwasawa 2007). The origin of the line in these systems is far from being understood. Matt et al. (1996) suggested that in obscured AGN, features from

<sup>4</sup> Coppin et al. (2010) also report a source redshift measurement of  $z = 4.751 \pm 0.005$  derived from a [OII]3727 emission line in a near-IR VLT spectrum, that is consistent with what is measured from the submm lines.

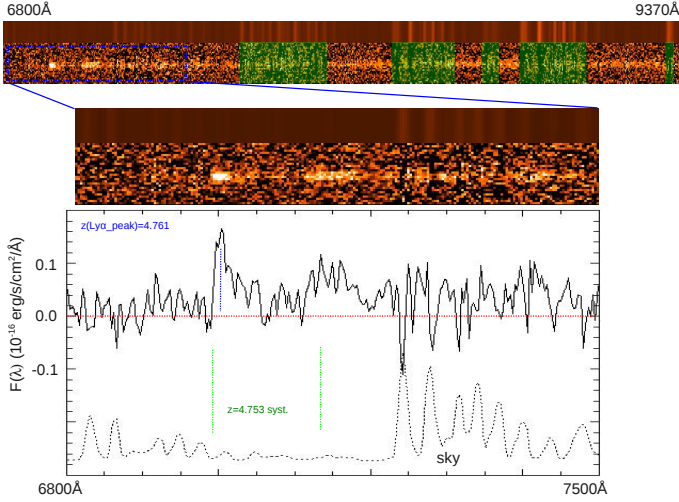


**Fig. 5.** The FORS2 two-dimensional spectrum is shown from 6800 to 9400 Å (top). The shaded green rectangles mark the noisy regions affected by intense sky emission lines. A zoom on the Ly $\alpha$  and N v positions in the wavelength interval 6800–7500 Å (blue dotted rectangle) is shown in the middle and bottom of the figure. The wavelength of the Ly $\alpha$  and N v at the systemic redshift derived from the [NII]205 $\mu$ m line (Nagao et al. 2012) are also reported (green vertical dotted lines).

highly ionized iron (ionization parameters  $\xi = 10^3 - 10^4$ ) could be produced by the so-called “warm mirror”, i.e. an optically thin plasma located on pc scales around the black hole. In local heavily obscured AGN, however, emission lines at 6.7–6.9 keV with  $EW \sim 1-2$  keV are far less common than the line at 6.4 keV, which is explained as fluorescent iron emission by an almost neutral reprocessor on the same pc scales, and are always accompanied by, and weaker than, the cold 6.4 keV line (in XID403 only loose constraints can be placed to the 6.4 keV line:  $EW \lesssim 4$  keV; Gilli et al. 2011).<sup>5</sup>

Nandra & Iwasawa (2007) suggested that the  $EW \sim 1$  keV line at 6.7 keV seen in the  $z = 0.3$  HyLIRG IRAS 00182-7112 might originate from a thin plasma which would be difficult to confine and should be then outflowing. Both the hidden QSOs in IRAS 00182-7112 and XID403 are indeed powerful enough to launch a plasma outflow driven by radiation pressure (Tombesi et al. 2013). Also, the luminosity of the Fe line in XID403 is of the same order of the X-ray luminosity expected for a 1000  $M_{\odot} \text{yr}^{-1}$  starburst (assuming the SFR vs  $L_x$  relations by Ranalli et al. 2003), and it is therefore unlikely that the starburst can provide enough photons at  $E > 8$  keV to ionize iron atoms up to Fe xxvi. It is nonetheless possible that both supernovae explosions and stellar winds excavate channels through the ISM making this plasma visible to the observer. This might explain why such strong lines from ionized iron are preferentially found in starburst galaxies.

If the detection of the  $\sim 6.9$  keV line in XID403 is real and it is associated to outflowing plasma, we can roughly estimate its mass outflow rate

<sup>5</sup> We note that the line at  $\sim 6.9$  keV rest-frame is unlikely to be a blue-shifted line at 6.4 or 6.7 keV rest-frame from Fe <xxvi, which would imply outflow velocities of  $\sim 23,000$  or  $\sim 9,000 \text{ km s}^{-1}$ , respectively, i.e. a factor of  $\sim 20 - 50$  larger than what is estimated from Ly $\alpha$ . While such ultra fast outflows (UFOs; e.g. Tombesi et al. 2013) of ionized gas have been seen in powerful AGN as absorption lines, they have never been observed in emission.

The line energy centred at  $\sim 6.9$  keV would imply a high ionization parameter  $\xi \sim 10^3 - 10^4$ , where

$$\xi = L_{ion}/(n_e R^2) \text{ erg cm s}^{-1}, \quad (5)$$

and  $L_{ion}$  is the source ionizing luminosity integrated between 13.6 eV and 13.6 keV (Tarter et al. 1969),  $R$  is the distance to the ionizing source, and  $n_e$  is the average electron density of the outflow.

In the case of a spherical or biconical geometry the outflow rate can be approximated with (McKernan et al. 2007):

$$\dot{M}_{out} \approx \mu_H n_e m_p \Omega R^2 v_{out}, \quad (6)$$

where  $\mu_H$  is the mean atomic mass per hydrogen atom,  $n_e$  is the average electron density of the outflowing plasma,  $m_p$  is the proton mass,  $\Omega$  is the solid angle subtended by the outflow ( $\Omega = 4\pi$  for a spherical outflow),  $R$  is the radius of the outflow (distance to the nucleus), and  $v_{out}$  the outflow velocity (here estimated through the Ly $\alpha$  shift). No clumpiness of the plasma is assumed. Solving Eq. 5 for  $n_e R^2$  and substituting into Eq. 6, returns:

$$\dot{M}_{out} \approx \mu_H m_p \Omega v_{out} L_{ion} / \xi. \quad (7)$$

By assuming  $\mu_H = 1.3$  (valid for solar abundances) and  $L_{ion} = L_{bol}/2$  (as measured from the average intrinsic QSO SED by Elvis et al. 1994) we obtained:

$$\dot{M}_{out} \approx 72 \left( \frac{\Omega}{4\pi} \right) \left( \frac{10^3}{\xi} \right) \left( \frac{v_{out}}{350} \right) M_{\odot} \text{yr}^{-1}. \quad (8)$$

The uncertainties on the estimated plasma outflow rate are admittedly large. In particular the rate would decrease for biconical outflows and ionization parameters  $\xi > 10^3$ . However, one may conclude that from a few to a few tens of  $M_{\odot}$  of highly ionized gas are expelled from the system every year. Observations of nearby AGN show that most of the outflowing mass is in a cool atomic or molecular phase rather than in a highly-ionized phase. For instance, Tombesi et al. (2012) measured plasma outflow rates of  $< 1 M_{\odot} \text{yr}^{-1}$  in a sample of local Seyfert 1 galaxies, while outflow rates of  $10 - 100 M_{\odot} \text{yr}^{-1}$  and  $100 - 1000 M_{\odot} \text{yr}^{-1}$  have been observed for neutral (Rupke et al. 2005) and molecular (Sturm et al. 2011) gas, respectively, in local ULIRGs hosting AGN of similar bolometric luminosity. Then, if we assume that also in XID403 most of the outflowing gas is molecular, the total mass of gas that is expelled may be of the same order of or even higher than that going into stars, as it is often observed in star forming galaxies with (Feruglio et al. 2010; Maiolino et al. 2012) or without (Newman et al. 2012; Bolatto et al. 2013) the presence of an AGN.

### 7.5. The descendants of XID403-like systems

The high SFR ( $1020 M_{\odot} \text{yr}^{-1}$ ) and the possibility that the outflow rate is similar to the SFR, suggest that XID403 will be depleted of all the available gas  $M_{gas} \sim 2.6 \times 10^{10} M_{\odot}$  in  $t_{dep} = M_{gas}/(SFR + \dot{M}_{out}) \approx 1.3 \times 10^7$  yr. Assuming that no further star formation would occur since then, XID403 would appear as an old, quiescent galaxy by  $z \sim 3$ , once its stellar populations have evolved for  $\sim 1$  Gyr. Coppin et al. (2009) showed that SMGs at  $z \sim 4 - 5$  possess the baryonic mass and gas depletion time-scales necessary to be the progenitors of luminous quiescent galaxies at  $z \sim 3$ , and that their space density is indeed consistent with that predicted by galaxy formation models. Based on our high-resolution submm observations with ALMA,

we here take a step further and suggest that objects like XID403 have also the right size to be the progenitors of quiescent galaxies at  $z \sim 3$ . Indeed, it has been shown (Daddi et al. 2005; Trujillo et al. 2007; Cimatti et al. 2008; van Dokkum et al. 2008) that a substantial fraction of passive galaxies at redshifts  $z > 1$  have sizes significantly smaller (a factor of 3 to 5) than local passive galaxies of equal mass, featuring stellar densities as high as  $\Sigma_* = (M_*/2)/(\pi r_{half}^2) > 10^{10} M_\odot \text{ kpc}^{-2}$  for ultra-compact systems (Cassata et al. 2011). One open question is how such old and compact remnants have formed. Very recently Barro et al. (2013) identified a population of compact star forming galaxies (cSFGs) at  $z = 2 - 3$ , whose number density, mass, size and star formation rates qualify them as likely progenitors of compact quiescent galaxies (cQGs) at  $z \sim 1 - 1.5$  (see also Williams et al. 2013). The incidence of nuclear activity in cSFGs is very high: about 30% of them appear to host an X-ray luminous AGN ( $L_x > 10^{43} \text{ erg s}^{-1}$ ), while the AGN fraction in non-compact star forming galaxies with similar mass and redshift is less than 1%. This suggests that AGN feedback may be responsible for a rapid evolution of star formation in cSFGs, leaving compact remnants on dynamical timescales ( $\sim 10^8 \text{ yr}$ ). XID403 appears to be similar to the cSFGs discussed by Barro et al. (2013) and hence to satisfy all the requirements to be the progenitor of a cQG at  $z \sim 3$ . The stellar density measured in XID403 (assuming  $r_{half} = 1 \text{ kpc}$ , as suggested by CANDELS data at  $2800\text{\AA}$  rest-frame) is  $\Sigma_* \sim 1.8 \times 10^{10} M_\odot \text{ kpc}^{-2}$ , comparable to that of ultra-compact galaxies at  $z > 1$ . At a rate of  $1020 M_\odot \text{ yr}^{-1}$ , its measured stellar mass of  $1.1 \times 10^{11} M_\odot$  must have been built in  $\sim 10^8 \text{ yr}$ , and it will grow at most by  $\sim 20\%$  ( $M_{*,end} = M_* + M_{gas} = 1.23M_*$ ) in the next  $\sim 10^7 \text{ yr}$ . This shows that most of the compact stellar core in XID403 is already in place. In addition, our ALMA data indicate that the vigorous star formation that is building that core *is* indeed happening on those sub-kpc scales, perhaps as a result of a major merger event (Hopkins et al. 2008) and/or direct feedback (first positive and then negative) from the hidden QSO (Zubovas et al. 2013).

## 8. Conclusions

We have reported ALMA Cycle 0 observations of the ULIRG XID403 at  $z = 4.75$  in the Chandra Deep Field South (CDFs). This system hosts the most distant Compton-thick QSO known to date and is an excellent laboratory to study the coevolution of a supermassive black hole with its host galaxy in the early Universe. We have complemented our sub-mm photometry with other data from ALMA and Herschel and built the far-IR SED of XID403. In addition, we took advantage of the dense UV to mid-IR coverage of the CDFS, and in particular of the CANDELS database, to build a broad band SED and obtain a spectral decomposition between the QSO SED and that of its host. We finally searched evidence of outflowing gas and re-analyzed the Chandra X-ray spectrum looking for Fe emission features associated to it. Our main results are the following:

- The source emission at 1.3 mm does not appear to be resolved in our ALMA data at  $\sim 0.75 \text{ arcsec}$  resolution. This places an upper limit of 2.5 kpc to the half-light radius of the continuum emission from dust heated by star formation. After deconvolving for the beam size, however, we found a  $\sim 3\sigma$  indication of an intrinsic source size of  $0.27 \pm 0.08 \text{ arcsec}$  (Gaussian FWHM), which would correspond to  $r_{half} \sim 0.9 \pm 0.3 \text{ kpc}$ . Further observations with ALMA at even higher resolution would fully resolve the source emission and hence accurately determine its physical size and properties.

- By fitting the far-IR SED with a modified blackbody spectrum we measured a warm dust temperature,  $T_d = 58.5 \pm 5.3 \text{ K}$ , that is comparable to what has been observed in other high- $z$  submillimeter galaxies. The star formation rate derived from the far-IR SED is  $\text{SFR} = 1020 \pm 150 M_\odot \text{ yr}^{-1}$ , in agreement with previous estimates at lower S/N. Based on the measured SFR and source size, we constrain the SFR surface density to be  $\Sigma_{\text{SFR}} > 26 M_\odot \text{ yr}^{-1} \text{ kpc}^{-2}$  ( $\Sigma_{\text{SFR}} = 200 M_\odot \text{ yr}^{-1} \text{ kpc}^{-2}$  for  $r_{half} \sim 0.9 \text{ kpc}$ ), similar to what is observed in other local and high- $z$  starburst galaxies.

- In the plausible assumption that both the molecular and atomic gas masses - derived from previous [CII] and CO(2-1) observations at low angular resolution - are co-spatial with dust and assuming  $r_{half} \sim 0.9 \pm 0.3 \text{ kpc}$ , we derived a column density of  $N_H \sim 0.3 - 1.1 \times 10^{24} \text{ cm}^{-2}$  towards the central SMBH. This is consistent with the column density of  $1.4_{-0.5}^{+0.9} \times 10^{24} \text{ cm}^{-2}$  measured from the X-rays. Therefore, in principle, if both gas and dust were confined within sub-kpc scales, this would be sufficient to produce the observed X-ray column density without any need of a pc-scale absorber (e.g. the torus postulated by Unified Models).

- We fitted the broad band SED of XID403 with a composite spectrum made of dusty simple stellar populations (SSPs) plus AGN emission reprocessed by hot dust. The optical and far-IR parts of the SED are well modeled by the direct and dust-reprocessed emission of stars, respectively. Hot-dust heated by the AGN is needed to fit the data at mid-IR wavelengths ( $4\mu\text{m}$  rest-frame). We measured a total stellar mass of  $1.1 \times 10^{11} M_*$  and an AGN bolometric luminosity of  $\sim 10^{46} \text{ erg/s}$ , which is about half of that produced by stars.

- We argued that most if not all of the UV/optical light in XID403 is produced by stars. On the one hand, an excellent fit to the smooth UV/optical SED is obtained just with stellar emission, without any need of an additional component. On the other hand, both the Ly $\alpha$  and N v emission features in the UV/optical spectrum can be ascribed to the strong starburst. In particular, the N v line, which is often regarded as an AGN signature, is in this case likely arising from stellar winds produced by hot and young (O) stars, as seen in local compact starbursts. If the AGN contribution to the UV/optical light is then negligible, the unresolved morphology in the HST/ACS z-band data would suggest that half of the stars could be located in a region even smaller than 0.3 kpc radius, providing an even stronger constraint to the system size.

- We speculated that the high compactness of star formation, together with the presence of a powerful AGN, likely produce an outflowing wind. This would be consistent with the  $\sim 350 \text{ km s}^{-1}$  velocity shift observed between the Ly $\alpha$  emission and the submm lines ([CII], CO(2-1), [NII]) and with the highly-ionized Fe emission line at  $\sim 6.9 \text{ keV}$  rest-frame tentatively observed in the X-ray spectrum. The forthcoming Chandra 3Ms exposure of the CDFS will almost double the X-ray photon statistics in XID403. This will provide an excellent opportunity to test the reality of the detected iron feature and constraint at best all physical parameters extracted from the current X-ray spectrum.

- Our analysis showed that a compact, potentially sub-kpc, stellar core, is already in place in XID403, with a stellar density similar to that of ultra-compact early type galaxies observed at  $z > 1$ . In particular, our high-resolution data from ALMA showed that the vigorous star formation that is building that core is indeed happening on the same sub-kpc scales. Besides the mass, star formation rate and gas depletion timescales, XID403 has then also the right size to be one of the progenitors of the compact quiescent massive galaxies seen at  $z \sim 3$ .

*Acknowledgements.* We thank Carlos De Breuck for sharing with us some of his unpublished ALMA results on XID403. The anonymous referee is acknowledged for useful comments. We acknowledge support from the Italian Space Agency under the ASI-INAF contract I/009/10/0 and from INAF under the contract PRIN-INAF-2012. FC acknowledges financial support from PRIN MIUR 2010-2011, project "The Chemical and Dynamical Evolution of the Milky Way and Local Group Galaxies", prot. 2010LY5N2T. This paper makes use of the following ALMA data: ADS/JAO.ALMA#2011.0.00716.S. ALMA is a partnership of ESO (representing its member states), NSF (USA) and NINS (Japan), together with NRC (Canada) and NSC and ASIAA (Taiwan), in cooperation with the Republic of Chile. The Joint ALMA Observatory is operated by ESO, AUI/NRAO and NAOJ.

## References

- Alexander, D. M., Smail, I., Bauer, F. E., et al. 2005, *Nature*, 434, 738  
 Barro, G., Faber, S. M., Pérez-González, P. G., et al. 2013, *ApJ*, 765, 104  
 Bianchi, S. 2013, *A&A*, 552, A89  
 Blain, A. W., Smail, I., Ivison, R. J., Kneib, J.-P., & Frayer, D. T. 2002, *Phys. Rep.*, 369, 111  
 Bolatto, A. D., Warren, S. R., Leroy, A. K., et al. 2013, *Nature*, 499, 450  
 Bongiorno, A., Merloni, A., Brusa, M., et al. 2012, *MNRAS*, 427, 3103  
 Bordoloi, R., Lilly, S. J., Hardmeier, E., et al. 2013, *ArXiv e-prints*  
 Bournaud, F., Dekel, A., Teyssier, R., et al. 2011, *ApJ*, 741, L33  
 Burtscher, L., Meisenheimer, K., Tristram, K. R. W., et al. 2013, *ArXiv e-prints*  
 Calura, F., Gilli, R., Vignali, C., et al. 2013, *MNRAS*, submitted  
 Calzetti, D., Armus, L., Bohlin, R. C., et al. 2000, *ApJ*, 533, 682  
 Capak, P., Carilli, C. L., Lee, N., et al. 2008, *ApJ*, 681, L53  
 Casey, C. M. 2012, *MNRAS*, 425, 3094  
 Casey, C. M., Chen, C.-C., Cowie, L., et al. 2013, *ArXiv e-prints*  
 Cassata, P., Giavalisco, M., Guo, Y., et al. 2011, *ApJ*, 743, 96  
 Chapman, S. C., Windhorst, R., Odewahn, S., Yan, H., & Conselice, C. 2003, *ApJ*, 599, 92  
 Cimatti, A., Cassata, P., Pozzetti, L., et al. 2008, *A&A*, 482, 21  
 Cisternas, M., Jahnke, K., Inskip, K. J., et al. 2011, *ApJ*, 726, 57  
 Comastri, A. 2004, in *Astrophysics and Space Science Library*, Vol. 308, *Supermassive Black Holes in the Distant Universe*, ed. A. J. Barger, 245  
 Conley, A., Cooray, A., Vieira, J. D., et al. 2011, *ApJ*, 732, L35  
 Coppin, K. E. K., Chapman, S. C., Smail, I., et al. 2010, *MNRAS*, 407, L103  
 Coppin, K. E. K., Smail, I., Alexander, D. M., et al. 2009, *MNRAS*, 395, 1905  
 da Cunha, E., Charlot, S., & Elbaz, D. 2008, *MNRAS*, 388, 1595  
 Daddi, E., Alexander, D. M., Dickinson, M., et al. 2007, *ApJ*, 670, 173  
 Daddi, E., Dannerbauer, H., Krips, M., et al. 2009, *ApJ*, 695, L176  
 Daddi, E., Elbaz, D., Walter, F., et al. 2010, *ApJ*, 714, L118  
 Daddi, E., Renzini, A., Pirzkal, N., et al. 2005, *ApJ*, 626, 680  
 De Breuck, C., Maiolino, R., Caselli, P., et al. 2011, *A&A*, 530, L8  
 Diamond-Stanic, A. M., Moustakas, J., Tremonti, C. A., et al. 2012, *ApJ*, 755, L26  
 Draine, B. T. & Li, A. 2007, *ApJ*, 657, 810  
 Elbaz, D., Dickinson, M., Hwang, H. S., et al. 2011, *A&A*, 533, A119  
 Elvis, M., Wilkes, B. J., McDowell, J. C., et al. 1994, *ApJS*, 95, 1  
 Engel, H., Tacconi, L. J., Davies, R. I., et al. 2010, *ApJ*, 724, 233  
 Feltre, A., Hatziminaoglou, E., Fritz, J., & Franceschini, A. 2012, *MNRAS*, 426, 120  
 Feltre, A., Hatziminaoglou, E., Hernán-Caballero, A., et al. 2013, *MNRAS*, 434, 2426  
 Feruglio, C., Maiolino, R., Piconcelli, E., et al. 2010, *A&A*, 518, L155  
 Förster Schreiber, N. M., Genzel, R., Bouché, N., et al. 2009, *ApJ*, 706, 1364  
 Fritz, J., Franceschini, A., & Hatziminaoglou, E. 2006, *MNRAS*, 366, 767  
 Fu, H., Jullo, E., Cooray, A., et al. 2012, *ApJ*, 753, 134  
 Geach, J. E., Hickox, R. C., Diamond-Stanic, A. M., et al. 2013, *ApJ*, 767, L17  
 Genzel, R., Tacconi, L. J., Gracia-Carpio, J., et al. 2010, *MNRAS*, 407, 2091  
 Gilli, R., Su, J., Norman, C., et al. 2011, *ApJ*, 730, L28  
 Greve, T. R., Vieira, J. D., Weiß, A., et al. 2012, *ApJ*, 756, 101  
 Guo, Y., Ferguson, H. C., Giavalisco, M., et al. 2013, *ApJS*, 207, 24  
 Heckman, T. M., Borthakur, S., Overzier, R., et al. 2011, *ApJ*, 730, 5  
 Hodge, J. A., Karim, A., Smail, I., et al. 2013, *ApJ*, 768, 91  
 Hopkins, P. F., Hernquist, L., Cox, T. J., & Kereš, D. 2008, *ApJS*, 175, 356  
 Iwasawa, K., Mainieri, V., Brusa, M., et al. 2012, *A&A*, 537, A86  
 Iwasawa, K., Sanders, D. B., Evans, A. S., et al. 2009, *ApJ*, 695, L103  
 Iwasawa, K., Sanders, D. B., Evans, A. S., et al. 2005, *MNRAS*, 357, 565  
 Iwasawa, K., Sanders, D. B., Teng, S. H., et al. 2011, *A&A*, 529, A106  
 Jaffe, W., Meisenheimer, K., Röttgering, H. J. A., et al. 2004, *Nature*, 429, 47  
 Jia, J., Ptak, A., Heckman, T. M., Braitto, V., & Reeves, J. 2012, *ApJ*, 759, 41  
 Juneau, S., Dickinson, M., Bournaud, F., et al. 2013, *ApJ*, 764, 176  
 Kennicutt, Jr., R. C. 1998, *ApJ*, 498, 541  
 Law, D. R., Steidel, C. C., Shapley, A. E., et al. 2012, *ApJ*, 759, 29  
 Leitherer, C., Chandar, R., Tremonti, C. A., Wofford, A., & Schaerer, D. 2013, *ApJ*, 772, 120  
 Lusso, E., Comastri, A., & Drissen, L. 1992, *ApJ*, 401, 596  
 Lindner, R. R., Baker, A. J., Beelen, A., Owen, F. N., & Polletta, M. 2012, *ApJ*, 757, 3  
 Lo Faro, B., Franceschini, A., Vaccari, M., et al. 2013, *ApJ*, 762, 108  
 Lusso, E., Comastri, A., Simmons, B. D., et al. 2012, *MNRAS*, 425, 623  
 Magdis, G. E., Daddi, E., Béthermin, M., et al. 2012, *ApJ*, 760, 6  
 Magnelli, B., Lutz, D., Santini, P., et al. 2012, *A&A*, 539, A155  
 Magnelli, B., Popesso, P., Berta, S., et al. 2013, *A&A*, 553, A132  
 Maiolino, R., Gallerani, S., Neri, R., et al. 2012, *MNRAS*, 425, L66  
 Matt, G., Brandt, W. N., & Fabian, A. C. 1996, *MNRAS*, 280, 823  
 McKernan, B., Yaqoob, T., & Reynolds, C. S. 2007, *MNRAS*, 379, 1359  
 McMullin, J. P., Waters, B., Schiebel, D., Young, W., & Golap, K. 2007, in *Astronomical Society of the Pacific Conference Series*, Vol. 376, *Astronomical Data Analysis Software and Systems XVI*, ed. R. A. Shaw, F. Hill, & D. J. Bell, 127  
 Menci, N., Fiore, F., Puccetti, S., & Cavaliere, A. 2008, *ApJ*, 686, 219  
 Murray, N., Quataert, E., & Thompson, T. A. 2005, *ApJ*, 618, 569  
 Nagao, T., Maiolino, R., De Breuck, C., et al. 2012, *A&A*, 542, L34  
 Nandra, K. & Iwasawa, K. 2007, *MNRAS*, 382, L1  
 Nardini, E. & Risaliti, G. 2011, *MNRAS*, 415, 619  
 Newman, S. F., Genzel, R., Förster Schreiber, N. M., et al. 2013, *ApJ*, 767, 104  
 Newman, S. F., Genzel, R., Förster-Schreiber, N. M., et al. 2012, *ApJ*, 761, 43  
 Nordon, R., Lutz, D., Shao, L., et al. 2010, *A&A*, 518, L24  
 Ostriker, E. C. & Shetty, R. 2011, *ApJ*, 731, 41  
 Petry, D. & CASA Development Team. 2012, in *Astronomical Society of the Pacific Conference Series*, Vol. 461, *Astronomical Data Analysis Software and Systems XXI*, ed. P. Ballester, D. Egret, & N. P. F. Lorente, 849  
 Pozzi, F., Vignali, C., Comastri, A., et al. 2010, *A&A*, 517, A11+  
 Pozzi, F., Vignali, C., Gruppioni, C., et al. 2012, *MNRAS*, 423, 1909  
 Ranalli, P., Comastri, A., & Setti, G. 2003, *A&A*, 399, 39  
 Rangwala, N., Maloney, P. R., Glenn, J., et al. 2011, *ApJ*, 743, 94  
 Rau, U. & Cornwell, T. J. 2011, *A&A*, 532, A71  
 Riechers, D. A., Bradford, C. M., Clements, D. L., et al. 2013, *Nature*, 496, 329  
 Riechers, D. A., Carilli, C. L., Maddalena, R. J., et al. 2011, *ApJ*, 739, L32  
 Rodighiero, G., Daddi, E., Baronchelli, I., et al. 2011, *ApJ*, 739, L40  
 Rupke, D. S., Veilleux, S., & Sanders, D. B. 2005, *ApJ*, 632, 751  
 Sanders, D. B. & Mirabel, I. F. 1996, *ARA&A*, 34, 749  
 Schinnerer, E., Carilli, C. L., Capak, P., et al. 2008, *ApJ*, 689, L5  
 Schmidt, M. 1959, *ApJ*, 129, 243  
 Simpson, J., Swinbank, M., Smail, I., et al. 2013, *ArXiv e-prints*  
 Solomon, P. M. & Vanden Bout, P. A. 2005, *ARA&A*, 43, 677  
 Steidel, C. C., Erb, D. K., Shapley, A. E., et al. 2010, *ApJ*, 717, 289  
 Sturm, E., González-Alfonso, E., Veilleux, S., et al. 2011, *ApJ*, 733, L16  
 Swinbank, A. M., Karim, A., Smail, I., et al. 2012, *MNRAS*, 427, 1066  
 Swinbank, M., Simpson, J., Smail, I., et al. 2013, *ArXiv e-prints*  
 Tacconi, L. J., Genzel, R., Smail, I., et al. 2008, *ApJ*, 680, 246  
 Tacconi, L. J., Neri, R., Chapman, S. C., et al. 2006, *ApJ*, 640, 228  
 Tarter, C. B., Tucker, W. H., & Salpeter, E. E. 1969, *ApJ*, 156, 943  
 Tombesi, F., Cappi, M., Reeves, J. N., & Braitto, V. 2012, *MNRAS*, 422, L1  
 Tombesi, F., Cappi, M., Reeves, J. N., et al. 2013, *MNRAS*, 430, 1102  
 Tristram, K. R. W., Meisenheimer, K., Jaffe, W., et al. 2007, *A&A*, 474, 837  
 Trujillo, I., Conselice, C. J., Bundy, K., et al. 2007, *MNRAS*, 382, 109  
 van Dokkum, P. G., Franx, M., Kriek, M., et al. 2008, *ApJ*, 677, L5  
 Vanzella, E., Cristiani, S., Dickinson, M., et al. 2008, *A&A*, 478, 83  
 Vanzella, E., Cristiani, S., Dickinson, M., et al. 2006, *A&A*, 454, 423  
 Vanzella, E., Pentericci, L., Fontana, A., et al. 2011, *ApJ*, 730, L35  
 Vieira, J. D., Marrone, D. P., Chapman, S. C., et al. 2013, *Nature*, 495, 344  
 Vignali, C., Piconcelli, E., Lanzuisi, G., et al. 2011, *MNRAS*, 416, 2068  
 Vignali, C., Pozzi, F., Fritz, J., et al. 2009, *MNRAS*, 395, 2189  
 Vito, F., Vignali, C., Gilli, R., et al. 2013, *MNRAS*, 428, 354  
 Walter, F., Decarli, R., Carilli, C., et al. 2012, *Nature*, 486, 233  
 Wang, R., Wagg, J., Carilli, C. L., et al. 2013a, *ApJ*, 773, 44  
 Wang, S. X., Brandt, W. N., Luo, B., et al. 2013b, *ApJ*, 778, 179  
 Weiß, A., De Breuck, C., Marrone, D. P., et al. 2013, *ApJ*, 767, 88  
 Williams, C. C., Giavalisco, M., Cassata, P., et al. 2013, *ArXiv e-prints*  
 Xue, Y. Q., Luo, B., Brandt, W. N., et al. 2011, *ApJS*, 195, 10  
 Zubovas, K., Nayakshin, S., King, A., & Wilkinson, M. 2013, *MNRAS*, 433, 3079